SCIENCE CHINA
Earth Sciences

• RESEARCH PAPER •

August 2015 Vol.58 No.8: 1387–1396
doi: 10.1007/s11430-014-5048-4

Connection of sea level variability between the tropical western Pacific and the southern Indian Ocean during recent two decades

WANG TianYu[1,2], DU Yan[1*], ZHUANG Wei[1] & WANG JinBo[3]

[1] *State Key Laboratory of Tropical Oceanography, South China Sea Institute of Oceanology, Chinese Academy of Sciences, Guangzhou 510301, China;*
[2] *University of Chinese Academy of Sciences, Beijing 100049, China;*
[3] *Scripps Institution of Oceanography, California 92093, USA*

Received October 21, 2014; accepted March 5 , 2015; published online April 8, 2015

Based on the merged satellite altimeter data and *in-situ* observations, as well as a diagnosis of linear baroclinic Rossby wave solutions, this study analyzed the rapidly rise of sea level/sea surface height (SSH) in the tropical Pacific and Indian Oceans during recent two decades. Results show that the sea level rise signals in the tropical west Pacific and the southeast Indian Ocean are closely linked to each other through the pathways of oceanic waveguide within the Indonesian Seas in the form of thermocline adjustment. The sea level changes in the southeast Indian Ocean are strongly influenced by the low-frequency westward-propagating waves originated in the tropical Pacific, whereas those in the southwest Indian Ocean respond mainly to the local wind forcing. Analyses of the lead-lag correlation further reveal the different origins of interannual and interdecadal variabilities in the tropical Pacific. The interannual wave signals are dominated by the wind variability along the equatorial Pacific, which is associated with the El Niño-Southern Oscillation; whereas the interdecadal signals are driven mainly by the wind curl off the equatorial Pacific, which is closely related to the Pacific Decadal Oscillation.

sea level/sea surface height, waveguide pathway, tropical Pacific, south Indian Ocean, interannual and interdecadal variabilities

Citation: Wang T Y, Du Y, Zhuang W, Wang J B. 2015. Connection of sea level variability between the tropical western Pacific and the southern Indian Ocean during recent two decades. Science China: Earth Sciences, 58: 1387−1396, doi: 10.1007/s11430-014-5048-4

Regional response to the global climate change has drawn increasing attentions in recent years. The thermal expansion and ice melting associated with the global warming continuously raise the global mean sea level (Milne, 2009). Understanding the future sea level changes would be very beneficial for the living safety of coastal and island residents. Although the global mean sea surface height (SSH) rises at about 3 mm a^{-1} since the 1990s, the rising rate is not globally uniform (Cazenave et al., 2002; Cazenave and Nerem, 2004; Carton et al., 2005). For example, during 1993–2012, the low-latitude west Pacific shows positive sea-level trends, while the east counterpart shows negative trends (Figure 1(a)). The most significant sea level rise occurs in the tropical West Pacific at a rate >10 mm a^{-1}. In the eastern part of south Indian Ocean (IO), SSH rises at about 5 mm a^{-1}. Tide gauge observations also show a significant sea level rise in the Indo-Pacific warm pool since the 1990s, which cannot be explained by the variability of El Niño/La Niña-Southern Oscillation (ENSO; Merrifield et al., 2012; Meyssignac and Cazenave, 2012). Regional SSH changes are not only associated with the changes of sea water temperature and salinity due to ice melting and surface heating, but also with other dynamical processes in the ocean. The combination of both of them induces complex spatial and

*Corresponding author (email: duyan@scsio.ac.cn)

temporal variations in SSH. Cabanes et al. (2006) pointed out that there are two major processes affecting interannual SSH variability: (1) The sea water specific volume changes driven by local sea surface buoyancy flux and wind-driven Ekman pumping; and (2) the barotropic and baroclinic oceanic adjustments due to Rossby wave propagation and quasi-stationary Sverdrup balance. Previous analyses suggested that the sea level rise in the Indo-Pacific warm pool is caused mainly by the increase of thermosteric height induced by the changes in the upper ocean heat content (Cheng et al., 2007, 2008; Qiu and Chen, 2012; Zhuang et al., 2013).

The Pacific and Indian Oceans occupy 70% area of the world's ocean and are connected by the Indonesian seas. The two ocean basins play an important role in global climate change. The Indo-Pacific warm pool dominates the changes of Walker cell and Hedley cell on interdecadal timescale and influences the Asia-Australian monsoon (Han, 2010). Furthermore, surface wind stress regulates the SSH in the warm pool by Ekman transport and convergence/divergence. The two oceans are also connected by the so-called "atmospheric bridge" resulting in a significant positive correlation of interannual SST variability between the tropical Indian Ocean and the eastern equatorial Pacific. This link is in a form of gear-type atmospheric coupling, triggering ENSO events when anomalous zonal winds occur over the equatorial IO (Wu and Meng, 1998). In addition, the Indonesian Through-flow (ITF) transports water from the tropical Pacific and thus influences the SSH variations in the southeast tropical IO (Gordon and Fine, 1996; Yu et al., 2003; Wu et al., 2010; Du and Fang, 2011). During the 1997–1998 El Niño event, the tropical IO and Pacific co-vary in both the SSH and the heat content, which can be partially explained by the impact of ITF transports (Wang et al., 2003). Previous studies pointed out that the Indonesian archipelago acts as an oceanic channel for the wave propagation from the tropical Pacific to the southeast IO (Clarke and Liu, 1993; Potemra, 2001; Feng et al., 2004; Wijffels and Meyers, 2004). These studies focused mainly on seasonal and interannual processes. In this paper, we investigate the wave propagation through the waveguide pathways in the Indonesian Seas on longer timescales. Particularly, we investigate the fast sea level rise in the past 20 years to establish the dynamic connection between the south IO and the west Pacific.

1 Data and methods

1.1 Sea surface height dataset

So far, the satellite altimeter observations have been carried out for more than 20 years. In this study, we use the gridded sea level anomalies (SLA) dataset distributed by the Collecte Localisation Satellites (CLS) Space Oceanographic

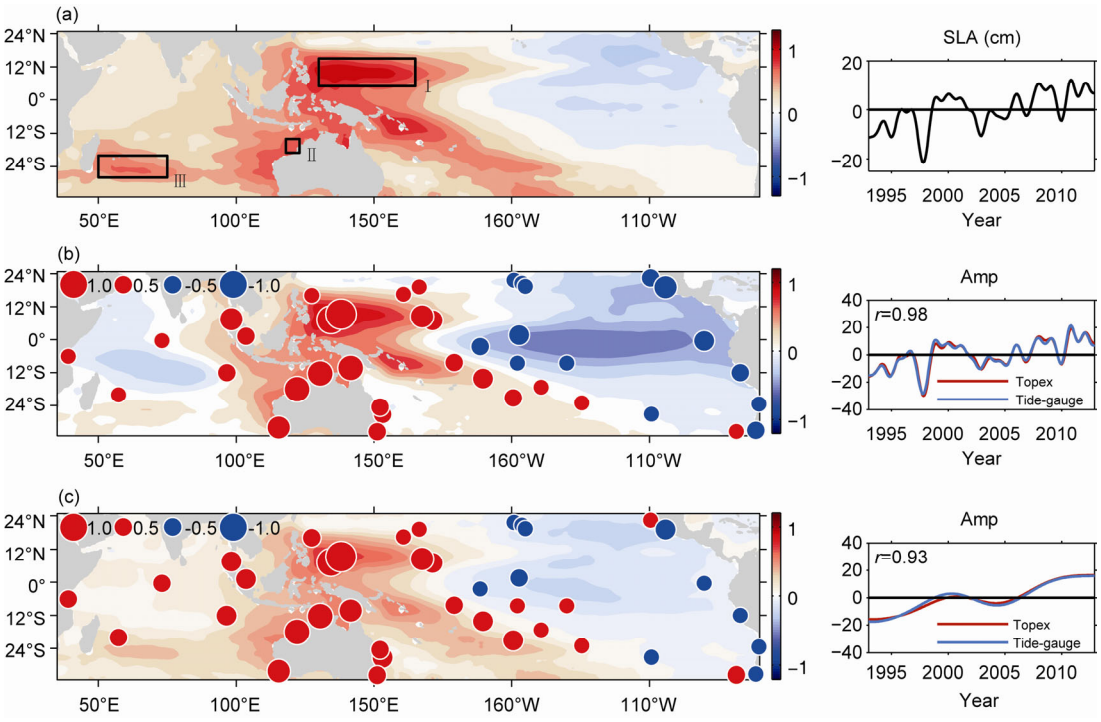

Figure 1 (a) Linear trend of altimetric SSH in 1993–2012 (cm a^{-1}, left) and the mean SSH anomaly (cm, right) within the box I (the east of Philippine Islands, 130°–145°E, 5°–15°N). (b) EOF-1 and PC-1 (mm) of monthly SLA observed by satellite altimetry (shading on left and red curves on right) and tide gauge stations (spots on left and blue curves on right). The climatological seasonal cycle and intraseasonal signals (<3 months) have been removed from the original data before the EOF analysis. (c) The same as (b), but for low-passed (>84 months) signals. The boxes II and III are defined in the regions off Northwest Australia (12°–16°S, 119°–123°E) and East of Madagascar (50°–75°E, 20°–28°S), respectively, which are used in the following figures.

Division of Toulouse, France. The dataset merges four altimeter observations together: Topex/Poseidon, Jason-1, ERS, and Envisat. The spatial resolution is 1/3° on a Mercator grid and the temporal resolution is weekly, covering the period from January 1993 to January 2013. Before further analyses, we average the dataset from weekly to monthly.

We also use the monthly records of total 40 tide gauge stations located in the tropical Pacific and Indian Ocean (30°E–90°W, 35°S–25°N) to further check the SSH changes (Figure1(b)). The dataset is provided by University of Hawaii Sea Level Center, USA. To investigate low-frequency sea level variations, the original dataset is averaged in a 13-month running window.

1.2 Temperature and salinity dataset

This study uses the monthly temperature and salinity dataset released by Ishii et al. (2006). The dataset merges the temperature and salinity profiles from World Ocean Data 2005 (WOD05), sea surface height data from COBE, temperature and salinity profiles from Argo, and Global Temperature and Salinity Professional Profiles (GTSPP, France). The product is available at 1°×1° spatial resolution and covers the period from January 1970 to January 2013. Vertically, the dataset extends from 0 to 1500 m and consists of 24 layers.

1.3 ECMWF ocean analysis system ORA-S3

ECMWF ORA-S3 is an operational ocean analysis/reanalysis system based on the Hamburg Ocean Primitive Equation model (Wolff et al., 1997) and the optimal interpolation assimilation. The system assimilates *in-situ* temperature and salinity profiles and altimeter sea surface height measurements (Balmaseda et al., 2008). We use the dataset with 1°×1° resolution, spanning from 1959 to 2009, available at Asia-Pacific Data-Research Center (APDRC), University of Hawaii.

1.4 Analysis methods

The Empirical Orthogonal Function (EOF) analysis, also called eigenvector analysis, is a method to extract principal components from a matrix (Pearson, 1902). EOF approach has been widely used in marine research since the Lorenz (1956) introduced it to meteorology and climate research. Because the EOF analysis is good at decomposing temporal and spatial signatures, we use it to analyze the Indo-Pacific SSH variations during 1993–2012. In addition, correlation and regression analysis are used to explore the links between SSH and sea surface wind stress to reveal the connections of wave propagation and air-sea interaction in different regions.

2 Results

2.1 Large-scale characteristics of SSH and SST variations

Using a least square method, we calculate the linear trend of SSH in Pacific and IO during 1993–2012 (Figure 1(a)). During this period, the tropical western Pacific and south IO show significant positive SSH trends with strong interannual variations, for example, over the tropical Pacific region (130°–165°E, 5°–15°N). The trend is relatively weak in the eastern Pacific. To further explore the spatial and temporal characteristics, we analyze the altimeter and tide gauge data using the EOF analyses (Figure 1(b)). The leading 10 EOF modes explain 82% and 88% of the total variance for the SST and SSH, respectively. The first mode accounts for 38% in tide gauge data and 55% in altimetry, which can roughly describe the low-frequency variations of SSH. The spatial pattern of EOF-1 shows a La Niña-like feature, high in the western and low in the eastern tropical Pacific. In the IO, the pattern shows high in the southern mid-latitude, with a slight high in the eastern part. In the time series, SSH peaks in the winters of 1997/1998, 2002/2003, 2006/2007, and 2009/2010, indicating the impact of El Niño events. To check the results without ENSO effect, we use a low-passing filter to extract the decadal signals with a period longer than 7 years from the original data and re-conduct the EOF analysis. As shown in Figure 1(c), EOF-1 of the decadal signals has a similar spatial pattern to that in Figure 1(a), accounts for 68% and 58% variances for altimeter and tide-gauge data, respectively. We expect that the PC-1 of decadal signals to show a linear SSH trend in the past 20 years. Besides, Figures 1(b)–(c) confirm that the SSH in the west Pacific and southwest IO is highly correlated in both the interannual and decadal timescales, which is consistent with previous studies (Wijffels and Meyers, 2004; Feng et al., 2010). It is worth noting that the PC-1s of altimeter and tide gauge data are highly correlated, with correlation coefficients 0.98 for original data and 0.92 for low-pass filtered data. This shows a high consistence between the two observational datasets.

In the tropical oceans, the anomalous steric height caused by temperature variation determines the SSH variation (Lombard, 2005; Cheng et al., 2007, 2008). This study analyzes the variability of surface (0 m) and subsurface (100–300 m average) temperature based on the Ishii dataset (Figure 2). During 1993–2010, the overall linear trends of surface and subsurface temperature are higher (lower) in the tropical western (eastern) Pacific. High SST trends are located mainly in the subtropical Pacific and the west coast of South America, implying the important roles of regional heat flux and air-sea feedback (Figure 2(a), Du and Xie, 2008), which differs from the SSH trend during the same period. Instead, the subsurface temperature trends are similar to the SSH trend, especially that the high trends reside in

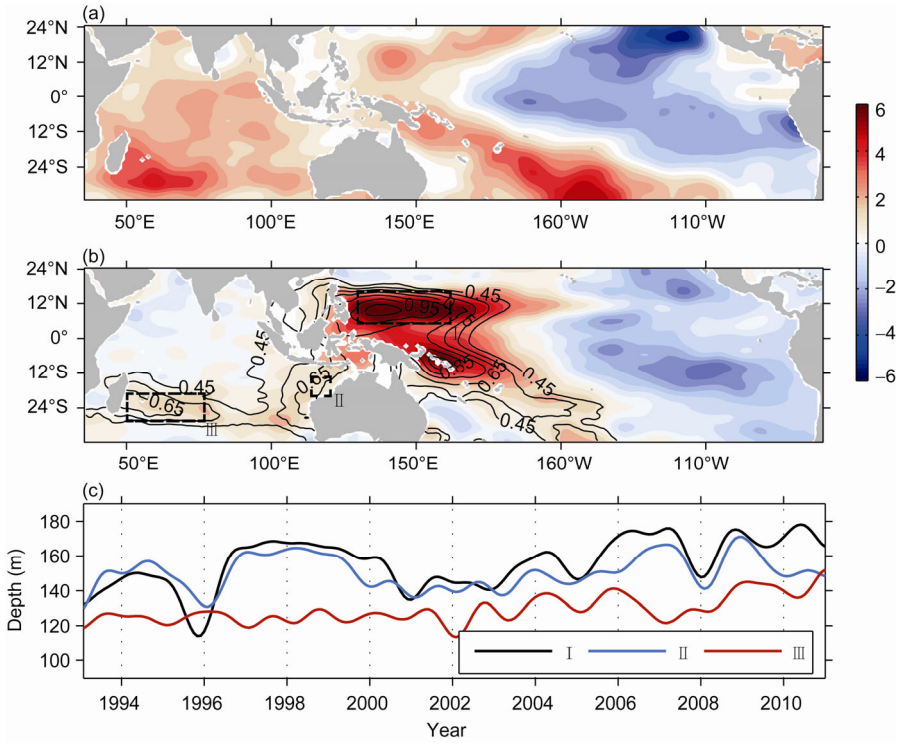

Figure 2 (a) Linear trend of Ishii sea surface temperature in 1993–2012 (°C a^{-1}). (b) The same as (a), but for sea subsurface temperature (°C a^{-1}, shading), and the linear trend of altimetric sea level (⩾0.45 mm a^{-1}, contours) as shown in Figure 1(a). (c) Low-frequency (with period >13 months) variability of 20°C isotherm depth in the three boxes as shown in Figure 1(a).

the tropical Pacific and South IO (Figure 2(b)). It implies that the thermocline adjustment should be a major factor for the SSH variations in the tropical Pacific and southeast IO. As shown in the previous studies, the rapid SSH rise in the west tropical Pacific in the late 1990s is dominated mainly by ocean dynamical processes, owing to the water convergences in the upper ocean (Cheng et al., 2008; Qiu and Chen, 2012). On the basis of the above spatial distribution of the SSH and subsurface temperature trends, we select 3 typical zones, east of Philippine Islands, northwest of Australia, and east of Madagascar, to check the temporal variability of the ocean temperature. Figure 2(c) shows that the time series of thermocline depth (20°C isotherm) in the Philippine Sea and to the northwest of Australia are consistent with each other, with a correlation coefficient of 0.84. But the thermocline depth variation to the east of Madagascar shows relatively weak amplitude and different phase from that in the Philippine Sea. The correlation coefficient is 0.36, indicating that the southwest IO and the tropical western Pacific are not directly linked (Masumoto and Meyers, 1998; Zhuang et al., 2013).

2.2 Wave pathways connecting the western Pacific and southern IO

The SSH changes reflect the baroclinic adjustment of thermocline (Figure 2(b); Cheng et al., 2008; Qiu and Chen, 2012). Planetary waves, as a form of baroclinic adjustment in the ocean, are often reflected in momentary undulations of sea level. At long timescale, the cumulative effects of high frequency wave lead to sustained changes in thermocline. Moreover, when the wave energy does not convert into heat dissipation completely, it increases the gravitational potential energy of seawater at the downstream of the wave and uplifts the sea level. So it is worth investigating the role of the wave dynamic in the tropical SSH changes. We select the northwest Australian coast (119°–123°E, 12°–16°S) as an indicator of the wave processes and construct an index of regional SSH variations. Then we calculate the 12-month lead-lag correlations between the defined SSH index and the entire SSH field. Figure 3 shows that the regions with correlations higher than 0.61 cover the South China Sea, Sulu Sea, Sulawesi Sea, Java Sea, Banda Sea, Timor Sea, northwest Australian coast, tropical Pacific, and New Guinea-Solomon Islands coast. Following these high-correlated areas, we get two belts as the waveguide pathways by linear fit (Figure 3). One pathway starts from the tropical north Pacific near 170°W, and extends along 10°N to the east of Mindanao, then reaches the coast of Australia across the Sulawesi Sea, Maluku Sea, and Banda Sea, finally ends in the east of Madagascar along 16°S. Another pathway starts from 170°W in the south Pacific, extends along the coast of New Guinea and Solomon Islands, and joins the first pathway in the Maluku Sea and further forward.

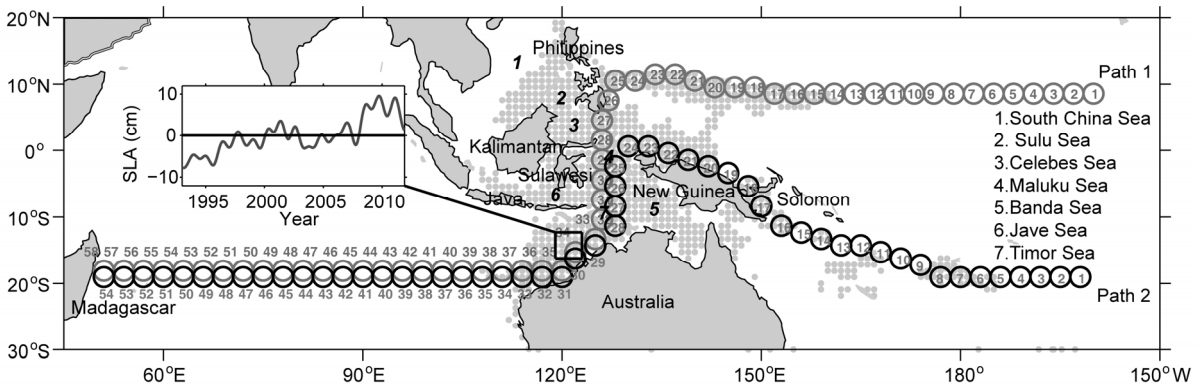

Figure 3 The estimated pathways for wave propagation (circles, Path A in gray and Path B in black). Gray dots indicate the locations with SSH significantly correlated (>95% confidence) with the target area (12°–16°S, 119°–123°E) based on the altimetric sea level dataset.

Along these two pathways, we analyze the low-frequency SSH signals. Figure 4(a) shows that the signals in the east part of the pathways change prior to the west part, indicating that the wave propagation is significantly westward. Generally, the wave propagation keeps its speed along the pathway in the same latitude. For example, the speeds between the tropical north Pacific to Mindanao (Figure 4(a) 1–25, left), between the tropical south Pacific to New Guinea (Figure 4(a) 1–17, right), and between the tropical southern IO 120° to 90°E (Figure 4(a) 35–44 left; Figure 4(a) 32–42, right) are about 0.21, 0.23, and 0.08 m s^{-1}, respectively, which agree well with the Rossby wave phase speed at those latitudes estimated by Radon transform method (Chelton and Schlax, 1996). However, it is worth noting that the westward wave propagation decays quickly after leaving Australia and strengthens again from the west of 100°E to the east coast of Madagassar Island. The break of wave propagation implies the importance of energy input in the interior southern IO. However, the simultaneous sea level changes around the Indonesian Seas imply a close connection among them. In the western Pacific, when Rossby waves reach Mindanao coast and east coast of New Guinea, they transform/excite Kelvin waves, which feature much faster wave speed and propagate to the Indonesian Seas and the southeast tropical IO (Yamagata et al., 1996). The large-scale wave adjustment processes are consistent with previous studies: Baroclinic Rossby waves from the tropical Pacific can excite Kelvin waves in the Indonesian Seas and the southeast tropical IO, which are reflected to become Rossby waves again along the northwest Australian coast and propagate westward into the south IO (Clarke and Liu, 1993; Potemra, 2001; Wijffels and Meyers, 2004).

2.3 Analyses of linear baroclinic Rossby wave model

In the open ocean, large-scale sea level variation can be largely explained by the westward propagating Rossby waves, either driven by wind-induced Ekman pumping or thermocline oscillation radiated from the eastern boundary (Meyers, 1979). As aforementioned, wave propagation in the tropical Pacific dominates the low-frequency SLA only in the southeast IO. It implies that the interior wind in the IO should be important to the SLA in the southwest IO. So we use the following linear vorticity equation (1) to investigate the relationship between wind, wave, and sea level variations:

$$\frac{\partial h}{\partial t}-c_R\frac{\partial h}{\partial x}=-\frac{g'\nabla\times\tau}{\rho_0 gf}-\varepsilon h, \tag{1}$$

where, h is baroclinic component of the SLA, c_R the zonal phase speed of the long baroclinic Rossby wave, g the gravitational constant, g' the reduced gravity, τ the anomalous wind stress vector, ρ_0 the density, f the Coriolis parameter, and ε the Newtonian damping coefficient, where 1/3 a^{-1} is adopted (Zhuang et al., 2013). Integrating eq. (1) westward from the eastern boundary (x_e) yields the solution:

$$\begin{aligned}h(x,y,t)=&h\left(x_e,y,t+\frac{x-x_e}{c_R}\right)\exp\left[\frac{\varepsilon}{c_R}(x-x_e)\right]\\&+\frac{1}{\rho_0 gh}\int_{x_e}^{x}\frac{g'}{c_R}\nabla\times\tau\left(x',y,t+\frac{x-x'}{c_R}\right)\exp\left[\frac{\varepsilon}{c_R}(x-x')\right]\mathrm{d}x'.\end{aligned} \tag{2}$$

The first and second terms on the right-hand side of eq. (2) represent SSH signals radiated from the eastern boundary and SSH signals induced by interior wind forcing, respectively (Capotondi and Alexander, 2001; Qiu, 2002; Zhuang et al., 2013). Merrifield (2011) studied whether the strengthen of tropical Pacific Ocean trade winds have impacts on regional sea level variations, and found that low-frequency winds (ORA-S3) can well explain the tropical Pacific SSH changes after 1993. Thus we use the low-frequency component in ORA-S3 wind as the forcing term in the eq. (2), and then calculate the SLA driven by both local wind and baroclinic Rossby wave along the pathways in Figure 3. Note that we cannot estimate the Kelvin wave propagation in the connection area between the

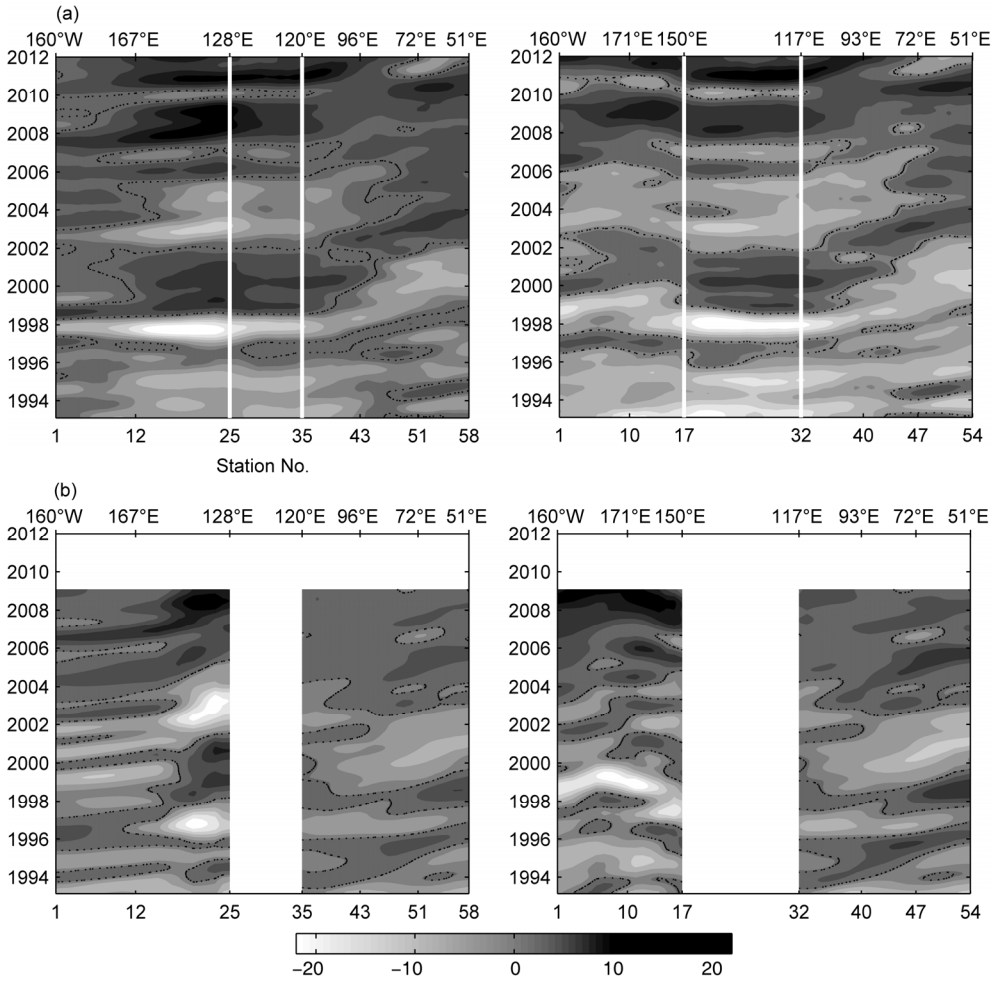

Figure 4 Time-station plot of low-frequency (with period >13 months) sea level variability (cm) along the two estimated pathways shown in Figure 3 for altimetric SSH (a) and modeled SSH (b) derived from linear baroclinic Rossby wave equation based on the ORA-S3 wind stress.

two oceans because the above method is only applicable to Rossby wave dynamics. So we construct a dumping coefficient α on the basis of observed SSH to estimate the portion of energy passing through the Indonesian Seas along the pathways. Here,

$$\alpha = \frac{\sum_{t=1}^{N} I_e(t) P_w(t)}{\sum_{t=1}^{N} P_w^2(t)},$$

with I_e representing the observed SSH anomaly west of Australia, P_w the observed SSH anomaly east of Mindanao. Therefore, we get the estimated h at the east boundary of the southern IO by $h(x_e, y, t) = \alpha \cdot h_w$ on the basis of the estimated h_w at the boundary of the west Pacific. As shown in Figure 4(b), the linear baroclinic Rossby wave model reproduces similar variations as the observations, such as the ENSO-like oscillations, the westward propagation, and the wave damping near 115°E. Moreover, the modeled signals are strengthened in the southwest IO, implying that the wind in interior IO is the key to sea level variations in the region (Masumoto and Meyers, 1998; Zhuang et al., 2013). Different SSH variability in the southeast and southwest IO explains the inconsistency of thermocline depth changes in these two regions (Figure 2(c)).

2.4 Interannual and interdecadal variations of the dynamic height in the Pacific

The variation of dynamic height reflects the change of the thermohaline structure in the ocean, and indirectly reflects the responses of sea water column to wind forcing and heat/fresh water exchange at the ocean surface (Willebrand et al., 1990; Glenn et al., 1991). The dynamic height is measured in dynamic meters and defined by $D(p_1, p_2) = \int_{p_1}^{p_2} \delta(T, S, p)\mathrm{d}p$, where P_1 and P_2 are two reference pressure levels, δ the specific volume anomaly, T the temperate, S the salinity, and P the pressure (Steven, 2004). Because the investigation of decadal variation needs a long-term dataset, we use the Ishii temperature and salinity

dataset, covering the period of 1970–2012, to estimate the sea surface dynamic height relative to 1000 m depth. We extract the interannual signal from original dynamic height using a 4–84 months band-pass filter and the interdecadal signal using a 7 years low-pass filter. Then we select northwest Australian coast (119°–123°E, 12°–16°S) as the target region to construct a dynamic height index, and make the same lead-lag correlation as in the Section 2.2. On the interannual timescale, the significant correlation (above 95% confidence level) occurs mainly over 10°S–10°N of the western Pacific basin and the eastern boundary of IO (Figure 5), indicating a domain of the activity of prevailing Rossby waves and Kelvin waves. The distribution of regression coefficients, high in the tropical western Pacific and low in the southeast tropical Indian Ocean, implies that the dynamical activity in the equatorial Pacific dominates the interannual variability in these regions. On the interdecadal timescale, significant correlations are located in the northern (2°–10°N) and southern tropical Pacific (15°–20°S). The maximum correlation occurs along latitude bands at 10°N and 20°S in Pacific and 18°S in IO, indicating the existence of the two waveguide pathways shown in Figure 3. Similarly, the regression coefficients show the dominated role of the dynamical activity in Pacific. Both of the figures show that the band at 10°N in the tropical Pacific is more important to the variability of the dynamic height in the southern IO.

We further analyze the pattern of global winds associated with the dynamic height index off the Northwest Australian coast. As shown in Figure 6, the wind pattern in the interannual time scale is significant in the central equatorial Pacific (Figure 6(a)), located in the eastern part of the region with high correlation in dynamic height (Figure 5(a)). The negative correlations of the zonal wind stress anomaly with the dynamic height index in the central equatorial Pacific imply that the enhanced trade wind along the equatorial Pacific increases the dynamic height/SSH in the tropical western Pacific, which might be associated with El Niño events (Bjerknes, 1969; An, 2008; Du and Qu, 2010). It suggests that the interannual dynamic height/SSH variation might be actually dominated by ENSO dynamics. On the interdecadal timescale, the dynamic height index is highly correlated with the wind anomalies off the equatorial Pacific as well as those along the central equatorial Pacific (Figure 6(b)). Besides, the negative (positive) wind stress curl in the northern (southern) hemisphere forces and maintains downwelling Rossby waves, which propagate westward and modulate the SSH variability in the Indo-Pacific warm pool region. Meanwhile, the distribution of wind associated with the positive decadal SSH signals is consistent with the wind pattern in the cold phase of Pacific Decadal Oscillation (PDO; Mantua et al., 1997), which might play a dominated role in the decadal SSH variations in the region.

To test the above hypothesis, we select two regions to average dynamic height, (130°–160°E, 5°S–5°N) in the equatorial Pacific to present interannual variability and

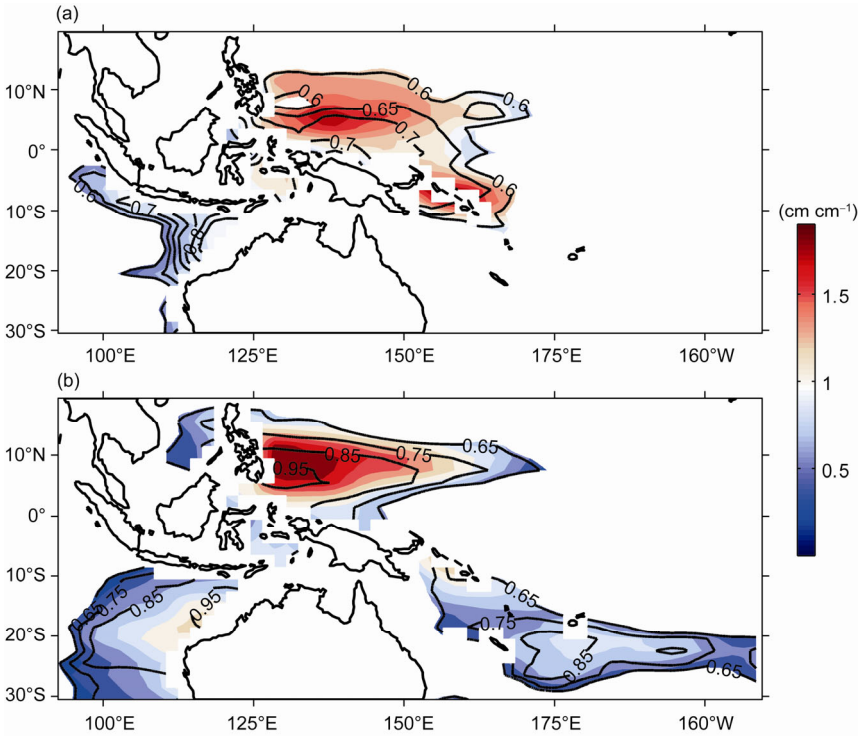

Figure 5 The significant lead-lag correlation coefficients (>95% confidence level, contours) and regression coefficients (shading) of dynamic height with the dynamic height index averaged in box II (12°–16°S, 119°–123°E) based on the Ishii temperature and salinity dataset for interannual (with period >4 months and <84 months (a), and interdecadal (with period >7 years) (b) timescales in the period of 1970–2009.

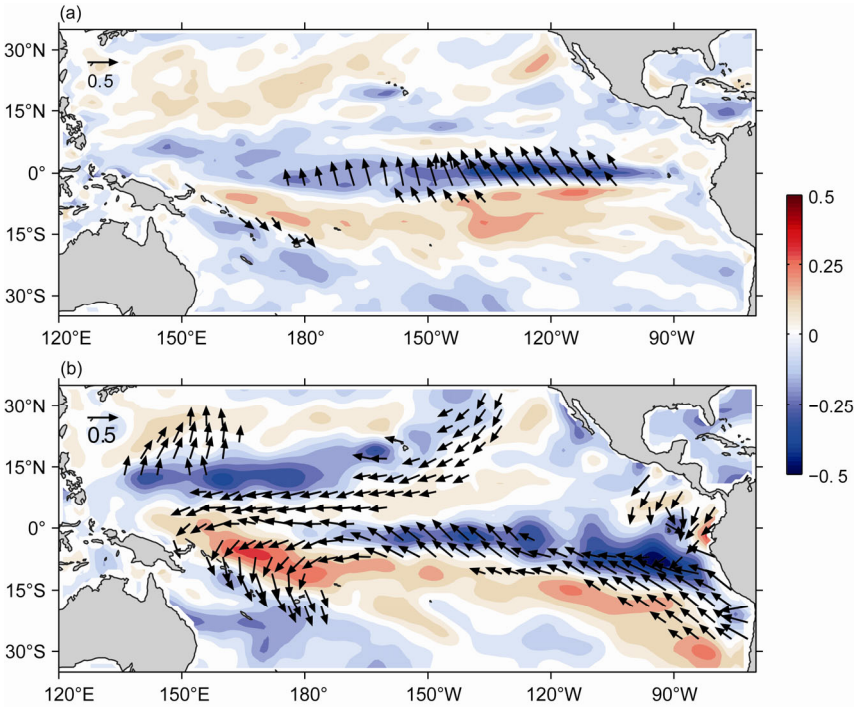

Figure 6 The wind stress (vectors) and wind stress curl (shading) that are significantly correlated (>95% confidence level) with the dynamic height index during 1970–2009 for interannual (a) and interdecadal (b) variabilities.

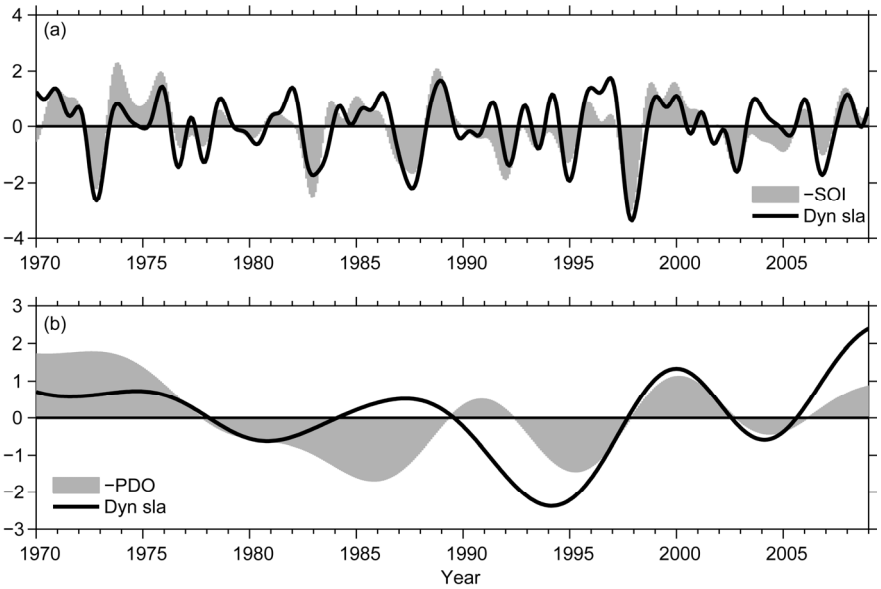

Figure 7 Standardized interannual (a) and interdecadal (b) dynamic height anomalies (curves). (a) Averaged in the west equatorial Pacific (5°S–5°N) and superimposed with the Niño 3.4 index (shading); (b) averaged in the west tropical Pacific (2°–10°N) and superimposed with the PDO index (shading).

(130°–165°E, 2°–10°N) in the north tropical Pacific to present interdecadal variability. Then we calculate the correlation between the dynamic height index and the Southern Oscillation index (SOI) and PDO index in the interannual and decadal time scales, respectively. The correlation coefficients reach –0.74 for interannual and –0.52 for interdecadal signals (Figure 7). It is worth noting that the correlation with the PDO index is robust after 1993 (Figure 7), implying the strengthening of PDO influence in recent 20 years.

3 Summary and discussions

Using multi-satellite altimeter measurements and *in-situ* tide

gauge observations, we examine the SSH variability on interannual and interdecadal timescales and reveal a dynamic link in SSH between the tropical western Pacific and the southeast Indian Ocean. The results show that the rapid SSH trend in the tropical western Pacific in recent 20 years is a part of the decadal variation and could have an impact on the southeast IO through the Indonesian Seas.

The lead-lag correlation analyses show that the low-frequency SSH variability in the southeast IO is affected mainly by the wave activities along 10°N and 16°S band within the Pacific basin. Along the pathways, we use a linear baroclinic Rossby wave solution to separate the influences of local and remote winds. We confirm that the low-frequency SSH variability in the southeast IO is dominated by the westward-propagating waves generated in the tropical Pacific, while that in the southwest IO is dominated by the local winds within the south IO.

The lead-lag correlation between global winds and the dynamic height index defined in the region off Northwest Australia reveals that the interannual and interdecadal wave signals have different propagation pathways and generation mechanisms. The interannual SSH variability is driven mainly by the wind stress anomalies in the equatorial Pacific, which is associated with the ENSO dynamics. On the other hand, the interdecadal SSH variability mainly attributes to the off-equatorial Rossby waves induced by the surface wind stress curl in the low-latitude Pacific, which is associated with the PDO. Especially, the connection between the interdecadal SSH signals and the PDO index increases after 1990s, which needs more specific analyses for its mechanism.

In this paper we mainly consider the Rossby wave pathways from the Pacific to the Indian Ocean. However, previous studies also found that westerly winds can excite equatorial Kevin waves propagating eastward along the Sumatra-Java coast to influence the circulation and SSH in the Indonesian Seas (Iskandar et al., 2005; Yuan, 2009). It remains a question whether this process has any impact on the connection between the Pacific and Indian Ocean in the decadal or longer timescale. More studies using *in-situ* data and numerical models are underway.

*This study benefits from discussions with Profs. Bo Qiu and Ruixin Huang. We thank the AVISO for providing satellite altimeter data (http://www.aviso.oceanobs.com), University of Hawaii Sea Level Center for tide gauge observations (*http://ilikai.soest.hawaii.edu/uhslc/data.html*). The Ishii temperature and salinity dataset was relisted by Frontier Research Center for Global Change (http://atm-phys.nies.go.jp/~ism/pub/ProjD/). The ECMWF ORA-S3 data were downloaded from the Asia-Pacific Data Research Center, University of Hawaii (http://apdrc.soest.hawaii.edu). This study was supported by the "Strategic Priority Research Program" of the Chinese Academy of Sciences (Grant No. XDA11010103), the National Basic Research Program of China (Grant Nos. 2012CB955603, 2010CB950302), and National Natural Science Foundation of China (Grant Nos. 41176024, 41176028). The research was also supported by the CAS/SAFEA International Partnership Program for Creative Research Teams.*

An S I. 2008. Interannual variations of the tropical ocean instability wave and ENSO. J Clim, 21: 3680–3686

Balmaseda M A, Vidard A, Anderson. 2008. The ECMWF Ocean Analysis System: ORA-S3. Mon Weather Rev, 136: 3018–3034

Bjerknes J. 1969. Atmospheric teleconnections from the equatorial Pacific. Mon Weather Rev, 97: 163–172

Cabanes C, Huck T, Verdiere A C. 2006. Contriburions of wind forcing and surface heating to interannual sea level variation in the Atlantic Ocean. J Phys Oceanogr, 36: 1739–1750

Capotondi A, Alexander M A. 2001. Rossby waves in the tropical North Pacific and their role in decadal thermocline variability. J Phys Oceanogr, 31: 3496–3515

Carton J A, Giese B S, Grodsky S A. 2005. Sea level rise and the warming of the oceans in the Simple Ocean Data Assimilation (SODA) ocean reanalysis. J Geophys Res, 110: C09006

Cazenave A, Bonnefond P, Mercier F. 2002. Sea level variations in the Mediterranean Sea and Black Sea from satellite altimetry and tide gauges. Glob Planet Change, 34: 59–86

Cazenave A, Nerem R S. 2004. Present-day sea level change: observations and causes. Rev Geophys, doi: 10.1029/2003RG000139

Chelton D B, Schlax M G. 1996. Global observations of oceanic Rossby waves. Science, 272: 234–238

Cheng X H, Qi Y Q. 2007. Trends of sea level variations in the South China Sea from merged altimetry data. Glob Planet Change, 52: 371–382

Cheng X H, Qi Y Q, Zhou W D. 2008. Trends of sea level variations in the Indo-Pacific warm pool. Glob Planet Change, 63: 57–66

Clarke R A, Liu X. 1993. Observations and dynamics of semiannual and annual sea levels near the eastern equatorial Indian Ocean boundary. J Phys Oceanogr, 23: 386-399

Du Y, Xie S P. 2008. Role of atmospheric adjustments in the tropical Indian Ocean warming during the 20th century in climate models. Geophys Res Lett, 35: L08712

Du Y, Qu T D. 2010. Three inflow pathways of the Indonesian throughflow as seen from the simple ocean data assimilation. Dynam Atmos Oceans, 50: 233–256

Du Y, Fang G H. 2011. Progress on the study of the Indonesian Seas and Indonesian Throughflow (in Chinese). Adv Earth Sci, 26: 1131–1142

Feng M, Li Y, Meyers G. 2004. Multidecadal variations of Fremantle sea level: Footprint of climate variability in the tropical Pacific. Geophys Res Lett, 31: L16302

Feng M, McPhaden M J, Lee T. 2010. Decadal variability of the Pacific subtropical cells and their influence on the southeast Indian Ocean. Geophys Res Lett, 37: L09606

Glenn S M, Porter D L, Robinson A R. 1991. A synthetic geoid validation of Geosat mesoscale dynamictopography in the Gulf Stream region. J Geophys Res, 96: 7145–7166

Gordon A L, Fine R A. 1996. Pathways of water between the Pacific and Indian oceans in the Indonesian seas. Nature, 379: 146–149

Han W Q. 2010. Patterns of Indian Ocean sea-level change in a warming climate. Nature, 3: 546–550

Ishii M, Kimoto M, Sakamoto K. 2006. Steric sea level changes estimated from historical ocean subsurface temperature and salinity analyses. J Oceanogr, 62: 155–170

Iskandar I, Mardiansyah W, Masumoto Y, et al. 2005. Intraseasonal Kelvin waves along the southern coast of Sumatra and Java. J Geophys Res, 110: C04013, doi: 10.1029/2004JC002508

Lombard A, Cazenave A, Le Traon. 2005. Contribution of thermal expansion to present-day sea-level change revisited. Glob Planet Change, 47: 1–16

Lorenz E N. 1956. Empirical orthogonal functions and statistical weather prediction. MIT Dept Meteorol, Sci Rept No 1. Cambridge: Statistical Forecasting Project Department of Meteorology

Mantua N J, Hare S R, Zhang Y. 1997. A Pacific interdecadal climate oscillation with impacts on salmon production. Bull Amer Meteorol Soc, 1069–1079

Masumoto Y, Meyers G. 1998. Forced Rossby waves in the southern tropical Indian Ocean. J Geophys Res, 103: 27589–27602

Merrifield M A. 2011. A shift in western tropical Pacific sea level trends during the 1990s. J Clim, 24: 4162–4138
Merrifield M A, Thompson P R, Lander M. 2012. Multidecadal sea level anomalies and trends in the western tropical Pacific. Geophys Res Lett, 39: L13602
Meyers, G. 1979. On the annual Rossby wave in the tropical North Pacific Ocean. J Phys Oceanogr, 9: 663–674
Meyers G, McIntonsh P, Pigot L. 2007. The Years of El Niño, La Niña, and Interactions with the Tropical Indian Ocean. J Clim, 20: 2872–2880
Meyssignac B, Cazenave A. 2012. Sea level: A review of present-day and recent-past changes and variability. J Geodyn, 58: 96–109
Milne G A. 2009. Identifying the causes of sea-level change. Nature Geosci, 2: 471–478
Pearson K. 1902. On the mathematical theory of errors of judgment, with special reference to the personal equation. Philos Trans R Soc A-Math Phys Eng Sci, 235–299
Potemra J T. 2001. Contribution of equatorial Pacific winds to southern tropical Indian Ocean Rossby waves. J Geophys Res, 106: 2407–2422
Qiu B. 2002. Large-scale variability in the midlatitude subtropical and subpolar North Pacific Ocean: Observations and causes. J Phys Oceanogr, 32:353–375
Qiu B, Chen S M. 2012. Multidecadal Sea Level and Gyre Circulation Variability in the Northwestern Tropical Pacific Ocean. J Phys Oceanogr, 42: 193–206
Steven K. 2004. Glossary of Physical Oceanography and Related Disciplines. Houston: Texas A&M University. 120–121
Wang D X, Liu Y, Liu Q Y. 2003. Connections in ocean upper layer between Indian Ocean and the west Pacific during 1997–1998 El Niño event. Chin Sci Bull, 48: 957–963
Wolff J, Maier-Reimer E, Legutke S. 1997. The Hamburg Ocean Primitive Equation model. Deutsches Klimarechenzentrum Tech Rep 13, Hamburg. 98
Willebrand J, Käse R H, Stammer D. 1990. Verification of Geosat sea surface topography in the Gulf Stream extension with surface drifting buoys and hydrographic measurements. J Geophys Res, 95: 3007–3014
Wu G X, Meng W. 1998. Gearing between the Indo-monsoon Circulation and the Pacific–Walker Circulation and the ENSO. PartI: Data Analyses (in Chinese). Sci Atmos Sin, 22: 470
Wu H Y, Li C Y, Zhang M. 2010. The preliminary numerical research of effects of ITF on tropical Pacific-Indian ocean associated temperature anomaly mode (in Chinese). J Trop Meteorol, 26: 513–828
Wijffels S, Meyers G. 2004. An Intersection of Oceanic Waveguides: Variability in the Indonesian Throughflow Region. J Phys Oceanogr, 34: 1232–1253
Yamagata T, Mizuno K, MasumotoY. 1996. Seasonal variations in the equatorial Indian Ocean and their impact on the Lombok throughflow. J Geophys Res, 101: 12465–12473
Yu Y Q, Zhou Z Y, Zhang X H. 2003. The impact on the climate when Indonesia hydrographic path shut down: A numerical simulation research. Chin Sci Bull, 48: 60–64
Yuan D L. 2009. Long wave dynamics of sea level variations during the Indian Ocean Dipole events. J Phys Oceangr, doi: 10.1175/2008JPO3900.1
Zhuang W, Feng M, Du Y. 2013. Low-frequency sea level variability in the southern Indian Ocean and its impacts on the oceanic meridional transports. J Geophys Res-Oceans, 118: 1302–1315